The role of the hydraulic resistance of the river bed and the time dependent response of the foundation layers in the assessment of water defences for macrostability and piping

Garuti, Dario; Jommi, Cristina; Rijkers, Richard

DOI
10.1007/978-3-319-99423-9_24

Publication date
2019

Document Version
Accepted author manuscript

Published in
Internal Erosion in Earthdams, Dikes and Levees

The role of the hydraulic resistance of the river bed and the time dependent response of the foundation layers in the assessment of water defences for macrostability and piping

Dario Garuti[1], Cristina Jommi[1*], Richard Rijkers[2]

[1] Delft University of Technology, Delft, The Netherlands
[2] Movares, Utrecht, The Netherlands
* c.jommi@tudelft.nl

Abstract: In the assessment of water defences for macrostability and backward erosion piping the design hydraulic load mostly refers to steady state conditions in equilibrium with the maximum river water level. In this contribution, we show selected results of coupled hydromechanical numerical analyses of a paradigmatic Dutch case, which demonstrate that this assumption leads to high overestimation of the true hydraulic loads at the toe of the water defence embankment. The hydraulic resistance of the bed of the river and the deformability of the foundation layers introduce a decay in the pore pressure time history, which largely reduce the action on the hydraulic protection structure. The finite element model was developed to assist in the assessment of an innovative solution based on passive wells as a measure to reduce the risk for macrostability and piping. It was calibrated on available pore pressure measurements in the foundation of critical sections of the dykes of the river Lek in the Netherlands under the daily tidal action. The model was used to determine the distribution of pore pressure expected in the subsoil of the dykes for the design maximum load. The calibration stage of the model is specifically interesting to the aim of evaluating the reduction of the input pore pressure due to the hydromechanical resistance of the geotechnical system.

Keywords: Dykes assessment, Numerical Analysis, Time dependent response, Water pressures

1. Introduction

Groundwater flow and pore water pressure build-up are known to be critical factors on the stability of river embankments. Among the failure mechanisms potentially affecting such retaining structures towards the inland, uplift and piping are a main concern, besides macro-instability of the embankment slopes (U.S. Department of Homeland Security 2016).

The ground conditions most critical to the occurrence of these types of mechanisms are those characterised by the presence of a permeable layer (aquifer) underlying a more impervious unit (aquitard), on top of which the embankment is built. When the permeable layer is in direct connection with the main water body, increases in water level of the latter may cause the aquifer water pressure to rise to a point where it might impair the stability of the embankment. This is not uncommon in fluvial environment, and the effects of uplift mechanisms were recognised in a wide range of cases, including rivers of remarkable size such as the Thames (Padfield, 1978) and the Danube (Grambalickova et al., 2005).

Among the remedial measures to counteract the pressure build-up, relief wells have been first employed by the U.S. Army Corps of Engineers by lowering the pressures under two dams (U.S. Army Corps of Engineers, 1992). These devices are meant to intercept the seepage water, relieve the pressures, and better control the flow and the discharge.

In the past, the design of relief wells has been based both on analytical and numerical approaches, and more than one method were proposed to evaluate a factor of safety for the functioning of the device (Guy et al. 2014). While analytical calculations (e.g. Barron 1982) are valuable in the case of simple geometry and isotropic soil conditions, a numerical solution is worthwhile in case of aquifer anisotropy, complex geometry and non-steady or transient analyses (e.g. U.S. Department of the Interior 2014). An instance of the employment of 2D Finite Element models to facilitate the design of relief well systems can be found in a case study analysed by Guy (2010).

In this contribution we analyse in detail the influence of hydromechanical coupling on the pore water pressure response of the subsoil of a paradigmatic river dyke, to evaluate the relevance of the hydraulic resistance of the river bed and of the compressibility of the subsoil layers on a reliable estimate of the pressure at the toe of the water defence embankment.

2. The Schoonhovenseveer-Langerak research project

The system of embankments under study lies on the left bank of the river Lek, in the Netherlands (Fig.1). This river is characterised by daily tidal fluctuations, and by relevant changes in the discharge due to seasonal precipitations. The variable hydraulic loads can be particularly detrimental on this site, due to the characteristics

of the local subsurface. While the first meters are composed of a relatively impervious Holocene clay layer, permeable shallow Holocene and deeper Pleistocene sand layers are found below the embankment, and these typically act as preferential paths for the water pressure fluctuations originating at the river (Movares and de Vries & van de Wiel, 2014a).

The major problem for the safety of the embankment analysed in this contribution is the macrostability of the inner slopes, which may be prone to failure along slip surfaces passing close to the dike toe (Movares and de Vries & van de Wiel, 2014b). However, in various other sections of the water defence system nearby, backward erosion piping is the main concern in the assessment (Fig.2).

One of the solutions developed to provide the necessary relief for water pressure is called “waterontspanner”, and consists of a system of vertical passive drain, encased in a PVC tube, equipped with a gravel filter layer (Fig. 3). The filter is installed in the permeable sand layer where most of the seepage under the embankment takes place, at a depth of approximately 10 m. In this way, the excess water can be conveyed though the drain, collected by a conduit at the top of the tube, and then discharged to a nearby drainage ditch, which runs parallel to the embankment (Fig. 4). On the upper end of the drain, a control device allows to adjust the value of the water pressure in the aquifer above which the drain starts functioning.

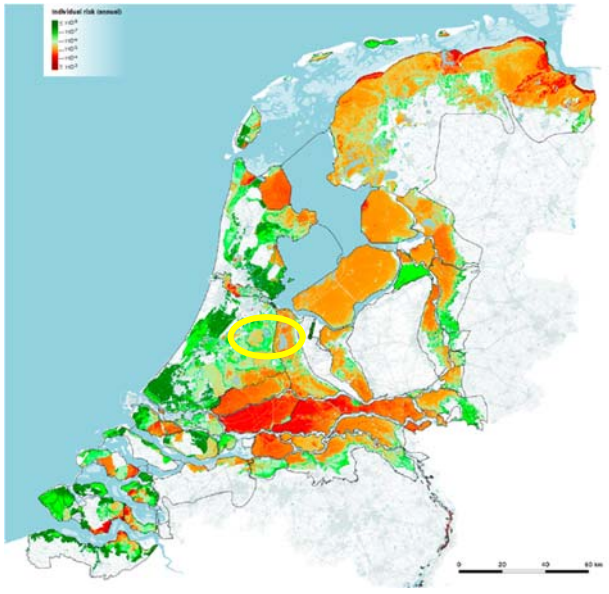

Fig. 1: Indication of the area under investigation

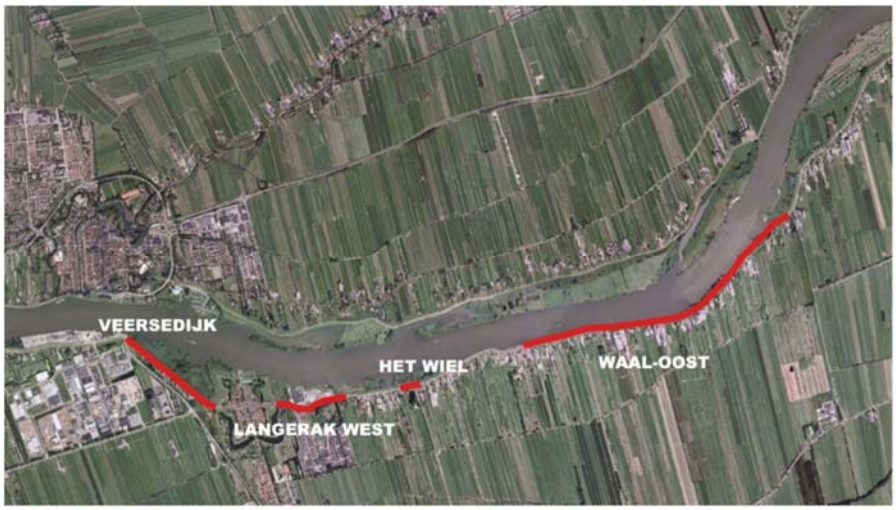

Fig. 2: Critical sections of the water defence system

The preliminary design procedure was based on the combination of pore water pressure results obtained by means of a finite-different software, MODFLOW, and stability calculations performed in 2D with D-Geo Stability, using Limit Equilibrium methods. The design high water wave was employed to simulate a high-water event with a return period of 2000 years. For each time step, the groundwater head profile was calculated by MODFLOW, and subsequently employed by D-Geo Stability to start Limit Equilibrium stability calculations.

Overlooking hydromechanical coupling neglects the stress-strain behaviour of the soil, and the influence that soil strains have on the hydraulic transmissivity. It should also be noted that a two-dimensional representation of the soil entails a great simplification of the properties of the subsurface, which is only representative of plain-strain conditions. In cases in which soil properties change considerably with respect to the longitudinal position along the embankment, the safety assessment is highly dependent on the choice of the section under study.

To gain better understanding of the dynamics behind the case under study, and provide more reliable estimates of the pore pressure history under after a high water event, a coupled hydromechanical 3D Finite Element model was developed on the PLAXIS 3D platform. The model carefully replicates local soil data and is calibrated on the available field information.

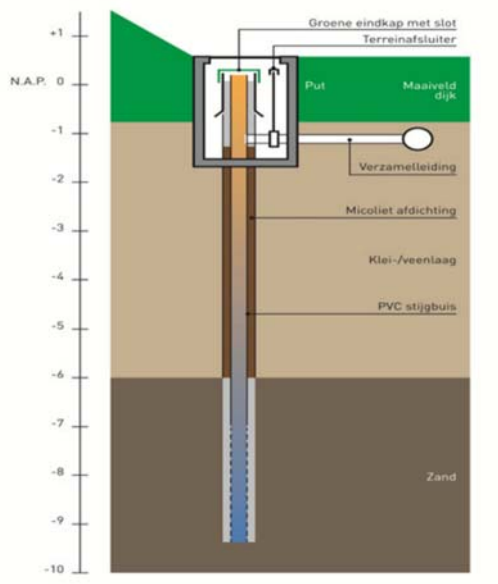

Fig. 3: Scheme of the passive well set up

Fig. 4: Scheme of the Waterontspanner system

3. Calibration of the model on field observation

The portion of the embankment chosen for the study is a 80 m x 80 m portion of the Veersedijk embankment (Fig. 5), centred around two observation wells (B99 and B100), which were employed in the calibration phase. Observation well B99 is located at the dike crest and B100 at a distance of 35 meters inland. Soil data from six boreholes were employed to describe the soil profile (Fig. 6). Soil characteristics for both the Holocene and Pleistocene aquifers and the interbedded clay and peat layers were obtained from a former site investigations and boreholes taken in locations nearby the embankment under investigation.

Fig. 5: Veersedijk, domain area and observation wells

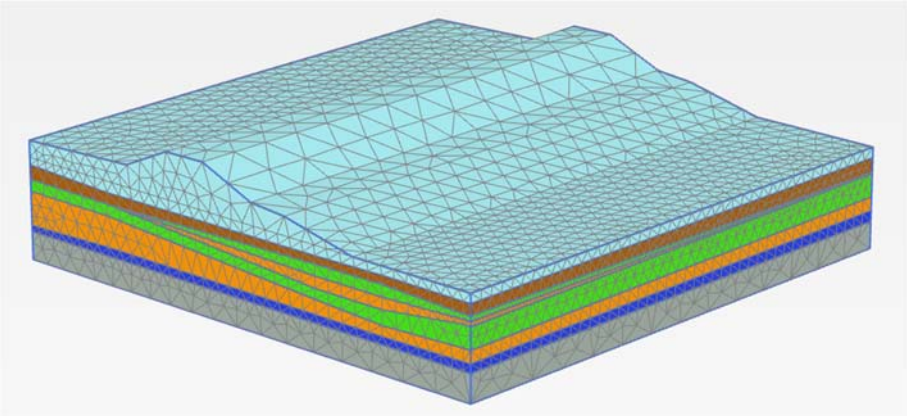

Fig. 6: 3D FE model of the Veersedijk

The calibration stage is based on field observations of tidal oscillations of the groundwater head retrieved from the two observation wells. The nature of the soil of the riverbed and of the interface between the river and the two aquifers is not known. The riverside boundary is separated from the river banks by a strip of land characterised by an irregular shape and variable width. No data were available for the water table far from the dyke on the polder side.

Groundwater head measurements for the Holocene and Pleistocene aquifers in the two observation wells B99 and B100 are shown in Fig. 7, together with the tidal fluctuations of the river level during the same time frame.

From the values of the groundwater head recorded in the two aquifers in B99, it can be observed that the amplitudes of the oscillations are reduced dramatically compared to the river level. This reduction is due to the hydraulic resistance of the river bed and the outer land. This decay observed between the river and well B99 is roughly the same in both aquifers.

However, the comparison between the readings in B99 and B100 in each single aquifer clearly shows that the amplitude of the pressure wave in the Holocene layer is further reduced towards the inland and delayed, while in the Pleistocene aquifer the decay and the decay are barely detectable. This suggests that the hydraulic conductivity of the Pleistocene sand is considerably higher than that of the Holocene layer, and that the compressibility of the upper layer plays a role too.

Based on these consideration, and in the absence of any detailed information on the river bed and outer land, it was decided to infer the pore pressure boundary conditions for the model on a back analysis of the measurements in the boreholes, which was performed using a simplified analytical solution for cyclic consolidation. The calibration was split in two phases: a stationary phase, in which constant head boundary conditions were applied to let the model equilibrate around the average

values observed in B99 and B100, and a time-dependent phase in which, both at the riverside and landside boundaries, fluctuating boundary conditions were applied.

In the time-dependent phase of the calibration, the boundary conditions applied on the riverside of the domain should include an intrinsic decay and delay with respect to the river level data. Conversely, the landside boundary condition should include a decay and delay with respect to the riverside boundary, governed by the soil characteristics assigned to the domain.

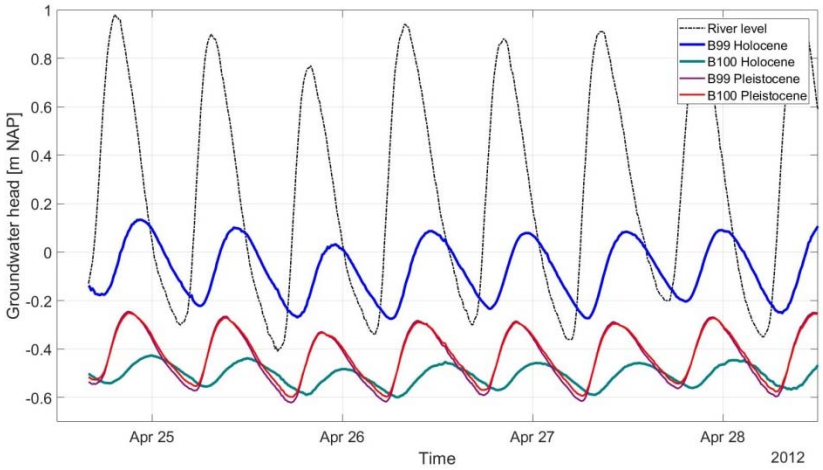

Fig. 7: Observed groundwater heads in B99 and B100

3.1 Boundary conditions and reduction factor

The simplified solution for cyclic consolidation in a river bed proposed by Barends (Baudin and Barends 1988) was used to backanalyse the response and assign the hydraulic boundary conditions to the numerical model. The solution was proposed for the typical Dutch river beds. However, it has been recently validated for the silty-sandy subsoil of different river dykes, where it proved to well capture pore pressure measurements (Jommi and Muraro 2014).

For a two-layered system of an aquifer and aquitard, the decay of the peaks amplitude H can be modelled with an exponential function of the distance x from a reference river section:

$$H(x) = H_0 \cdot e^{-\left(\frac{x}{\lambda_\omega}\right)} \tag{1}$$

where λ_ω is a function of the hydraulic conductivities (k, k_0) and of the compressibilities of the aquifer and aquitard.
Similarly, for the decay of the amplitude between two points x_A and x_B

$$\frac{H(x_B)}{H(x_A)} = e^{-\left(\frac{x_B - x_A}{\lambda_\omega}\right)} \tag{2}$$

The delay between the peaks in x_A and x_B can be expressed as a linear function of the distance:

$$\Delta t_{A\to B} = \frac{a(x_B - x_A)}{\omega\lambda_\omega} \tag{3}$$

where ω is the angular frequency of the fluctuations and a is a function of the hydraulic conductivity and of compressibility of the two soil units.

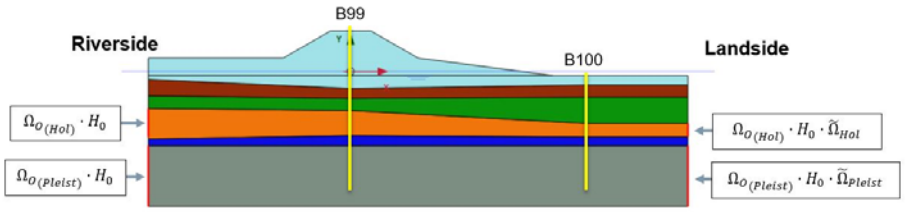

Fig. 8: Scheme of the groundwater head boundary conditions

The time-dependent phase of the calibration consists in detecting the dynamic boundary conditions on the outer and inner boundaries of the Holocene and Pleistocene sand layers. Such boundary conditions are characterised by a time dependent head fluctuation $\Delta h(t)$ around the mean value resulting from the stationary phase. The functions describing such fluctuations are indicated as $\Delta h_0(t)$ for the outer (riverside) and $\Delta h_0(t)$ for the inner (landside) boundary (Fig. 8). In both cases, the function is chosen to be proportional to the measured river level on the Lek $\Delta h_L(t)$. It should be noted that, for both boundary conditions, a decay Ω and a delay ϕ with respect to the river must be introduced:

$$\Delta h_O(t) = \Omega_O \cdot \Delta h_L(t - \phi_O) \tag{4}$$

$$\Delta h_I(t) = \Omega_I \cdot \Delta h_L(t - \phi_I) \tag{5}$$

If we substitute $t' = t - \phi_I + \phi_O$ in the first equation, a straightforward result is that:

$$\Delta h_I(t) = \tilde{\Omega} \cdot \Delta h_O\left(t - \tilde{\phi}\right) \tag{6}$$

$$\tilde{\Omega} = \frac{\Omega_I}{\Omega_O} \quad , \quad \tilde{\phi} = \phi_I - \phi_O \tag{7}$$

Therefore, if a reduction factor with respect to the river level is chosen for the outer boundary condition, the same factor should also be applied to the inner boundary condition.

The expected delays and decays between the two boundaries, separated by a distance of 80 m, was calculated via the analytical solution, written for the local soil properties. The results showed that an optimal value for the reduction factor Ω_O was equal to 0.5 for both aquifers. The fact that the same factor is suitable for both aquifers, shows that the river bed resistance acts in a similar way on the two layers. The result of the calibration stage are shown in Fig. 9 and Fig. 10.

The results in Fig. 9 and Fig. 10 show that a remarkable accordance could be achieved for the Holocene aquifer. Instead, for the Pleistocene aquifer, the nearly undetectable decay between the two boreholes was far less satisfactory. However, due to the fact that the Pleistocene aquifer is far less crucial to the stability of the structure, the back analysis was not refined further.

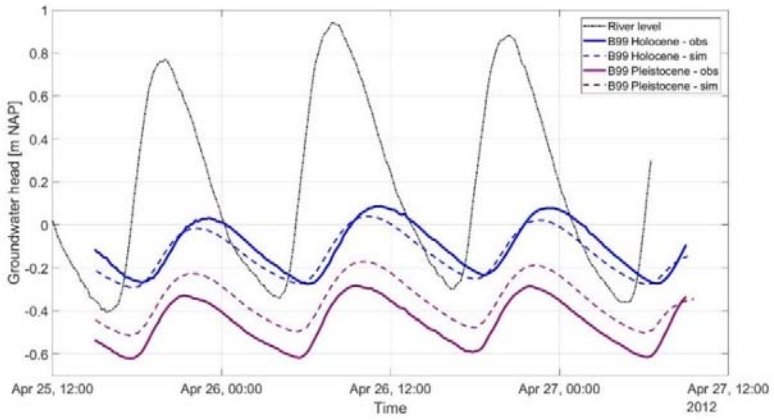

.

Fig. 9: Simulated and observed groundwater heads in B99

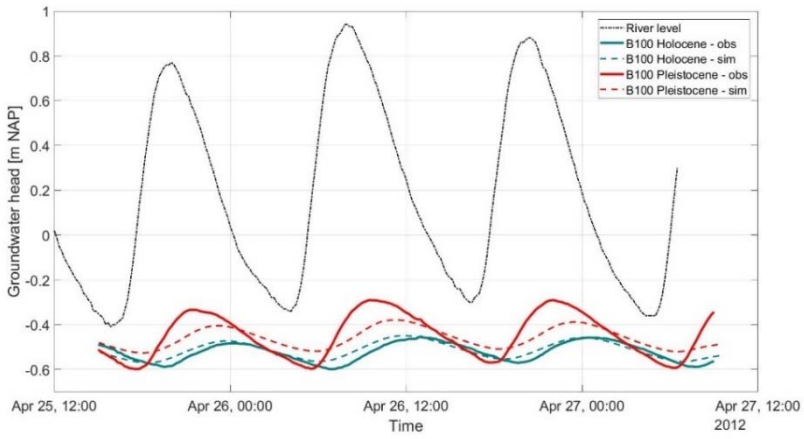

Fig. 10: Simulated and observed groundwater heads in B100

4. Selected numerical results

4.1 Preliminary 2D analyses

Numerical analyses were performed to assess the response of the system to the Design High Water wave. Preliminarily, a 2D plane strain section of the dyke was employed to address the following issues: establishing the most critical time of the high-water wave for the stability of the structure, examining the influence of the distance between the drain system and the embankment, providing a sketch of the failure mechanism. To assess the consequences of the pore pressure oscillation on this dyke section, the factor of safety (FoS) against macrostability was calculated by means of the strength reduction method (e.g. Griffiths et al 2007, Vaughan et al 2008).

The evolution over time of the FoS in Fig. 11 allows highlighting that the response of the system, even for aquifers with relatively high hydraulic conductivity, is clearly time dependent, and that the most critical conditions typically follow the peak of the high water event with a considerable delay. In the case analysed, the dip in the FoS is predicted to occur with a delay of 2 days, proving that time dependent behaviour of the soil should be considered when choosing the most critical time for the stability calculations. The shape of the associated failure surface (Fig. 12) shows the influence of underpressures at the toe, with a failure mechanisms extending beyond the toe for an overall length of roughly 30 m.

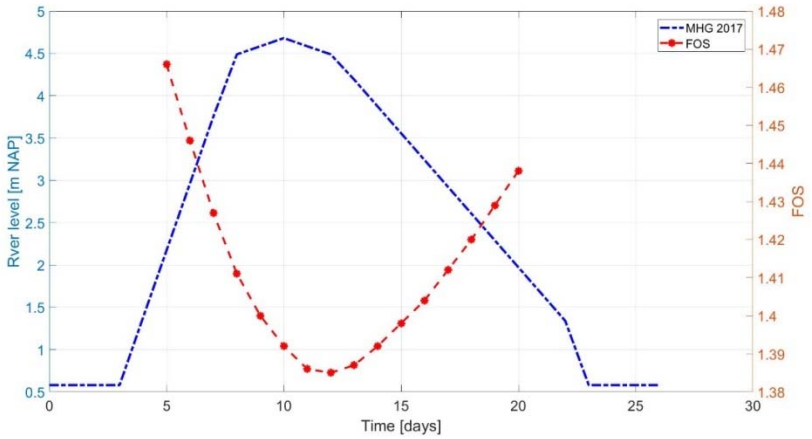

Fig. 11: Time evolution of the FoS during the simulated design high water event

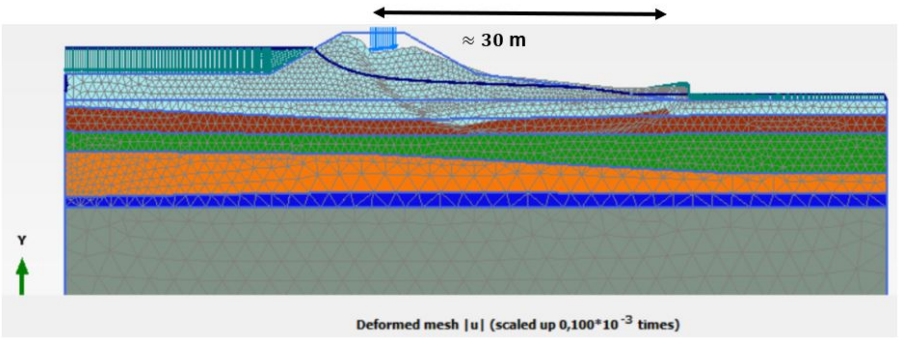

Fig. 12: Predicted failure mechanism (2D-analysis)

4.2 3D pore pressure distribution

Some aspects of the design of a system of relief wells was studied analysing the displacements, the factor of safety against macrostability and the pore water pressure distribution. Selected results of the latter aspects are summarised in the following due to their relevance for the global response of the system, possibly including backward erosion piping staring at the toe. The number of drains in the domain was increased from three to eight, corresponding to a spacing decreasing from 27 m to 10 m. The horizontal distance from the dike body was kept equal to 20 m, roughly equalling three times the height of the structure.

If a longitudinal section is taken at the drains location and the drawdown plotted for the Holocene aquifers (Fig. 13), a pattern of peaks and dips is visible, whose height clearly depends on the spacing between the drains.

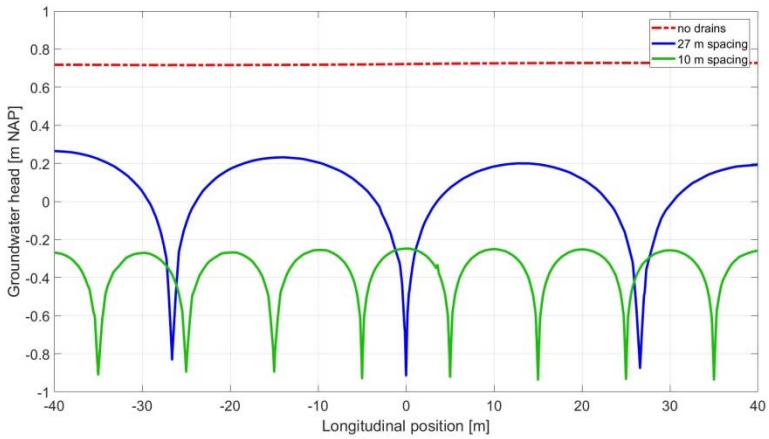

Fig. 13: Longitudinal profile of the highest ground water head following the design high water at the drains location

A useful insight on what happens in the subsoil of the embankment can be obtained by drawing two transversal sections: one corresponding to a drain location, and the other taken midway between two drains. On the transversal section including a drain (Fig. 14) the drawdown profiles always lie between the one corresponding to the pore pressure profile obtained without drains, and the limiting maximum one obtained with a 2D simulation, which obviously overestimates the efficiency of the true system.

Figure 15 shows that efficiency of the drains system is not limited to the location where the drains are installed. In the area closer to the embankment, where the effects of the drawdown are the greatest, the results show that there is no significant difference in the drawdown observed between the two sections of Fig. 14 and Fig. 15. It appears therefore that the effect of the drains, despite being longitudinally non-uniform at the location of the screens, flattens out in proximity of the dike, resulting in a mitigating effect on the excess pore water pressure that does not markedly depend on the longitudinal coordinate.

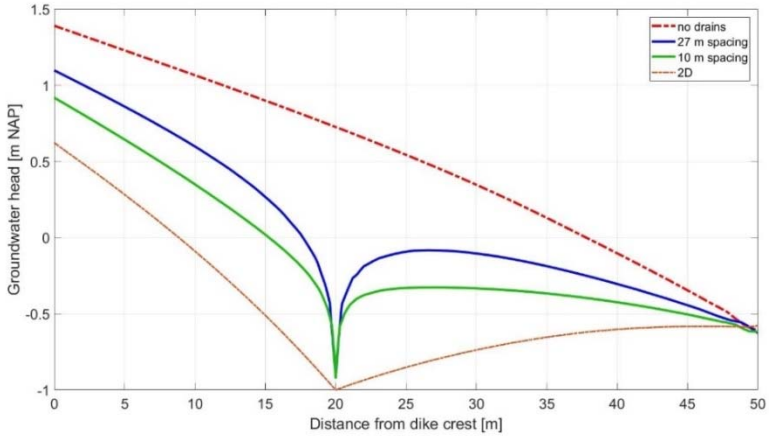

Fig. 14: Groundwater head profile at drain location - transversal section

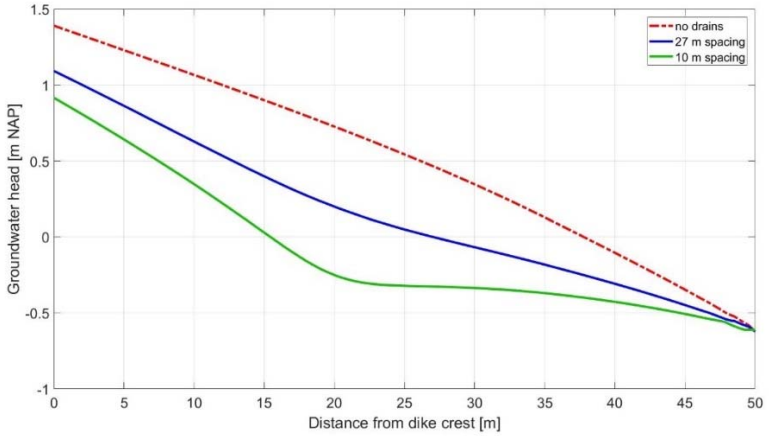

Fig. 15: Groundwater head profile between two drains - transversal section

5. Conclusions

The numerical exercise was set up to assess a possible technical solution designed to increase the factor of safety of river dykes by means of passive wells at the toe. The solution is being studied for the improvement of critical dyke sections both for macrostability and backward erosion piping.

To the aim of design and assessment, a time-dependent coupled analysis appears to be crucial to avoid overestimating the pore pressure which enter in the calculation. The river bed hydraulic resistance can be quite high reducing to a large extent the forcing hydraulic head. In the upper sandy aquifers, the compressibility plays a role too in attenuating the pressure wave affecting the subsoil.

The individual contribution of these aspects is not immediate to assess. However, a thorough backanalysis of multilevel piezometer readings will help in calibrating numerical models set up to predict the response of the water defence under high water events. Especially the river bed resistance is typically unknown, and the results of the analyses presented suggest that better characterisation of the area will help in more reliable assessment of water defences, hence better addressing reinforcement efforts.

References

Baudin CMHLG, Barends FBJ (1988). Getijde-respons in grondwater onder Nederlandse dijken, H_2O 21 (1), 2-5.

Barron R (1982). Mathematical Theory of Partially Penetrating relief wells, (1982).

Grambalickova D, Bednarova E (2005). Some aspects of the safety of flood embankments, Slovak Journal of Civil Engineering.

Griffiths DV, Marquez R (2007) Three-dimensional slope stability analysis by elasto-plastic finite elements, Géotechnique 57, 537-546.

Guy ED (2010) Relief well system design approach: Hhd case study, Association of State Dam Safety Officials Proceedings, Charleston,West Virginia.

Guy ED, Ider HM, Darko-Kagya K (2014) Several relief wells design considerations for dams and levees, 45th Annual Ohio river valley soils Seminar.

Jommi C, Muraro S (2014). The geotechnical response of dykes and levees to hydraulic loads (in Italian). Panel contribution. La Geotecnica nella Difesa del Territorio e delle Infrastrutture dalle Calamità Naturali, XXV National Geotechnical Conference, Baveno, Italy

Movares, de Vries & van deWiel (2014a) Achtergrondrapport geohydrologie.

Movares, de Vries & van deWiel (2014b) Ontwerpnota.

Padfield CJ (1978) The stability of river banks and flood embankments, Ph.D. thesis, University of Cambridge.

U.S. Department of Homeland Security (2016) Training aids for dam safety: Evaluation of seepage conditions.

U.S. Army Corps of Engineers (1992) Design, Construction and Maintenance of Relief Wells.

U.S. Department of the Interior (2014) Embankment Dams (Ch 21): Water removal and control: dewatering and unwatering systems.

Vaughan P, Griffiths DV, Marquez R (2008) Authors' reply, Géotechnique 58, 683-685.